

Theoretical study of electron-ion resonant recombination of Be-like Si^{10+} ion

Jing-Lin Rui(芮静琳), Jian-Ping Pan(潘建平), Lu-You Xie(颉录有), Yu-Long Ma(马玉龙), and Chen-Zhong Dong(董晨钟)

Citation: Chin. Phys. B, 2026, 35 (**3**): 033402. DOI: 10.1088/1674-1056/ae2f54
http://cpb.iphy.ac.cn; http://iopscience.iop.org/cpb

What follows is a list of articles you may be interested in

Experimental study on the vibrational relaxation mechanism of $N_2(X^1\Sigma_g^+, v = 6)$ molecules in collision with N_2, O_2, and CO

Yaqi Zhang(张亚琦), Yuhao Wu(武宇豪), Jing Liu(刘静), Jiaxin Lin(林佳欣), and Maofu Yu(于茂福)
Chin. Phys. B, 2026, 35 (**3**): 033401. DOI: 10.1088/1674-1056/adf82e

Theoretical investigation of electron-impact ionization of W^{8+} ion

Shiping Zhang(张世平), Fangjun Zhang(张芳军), Denghong Zhang(张登红), Xiaobin Ding(丁晓彬), Jun Jiang(蒋军), Luyou Xie(颉录有), Yulong Ma(马玉龙), Maijuan Li(李麦娟), Marek Sikorski, and Chenzhong Dong(董晨钟)
Chin. Phys. B, 2024, 33 (**3**): 033401. DOI: 10.1088/1674-1056/ad1487

Atomic structure and collision dynamics with highly charged ions

Xinwen Ma(马新文), Shaofeng Zhang(张少锋), Weiqiang Wen(汶伟强), Zhongkui Huang(黄忠魁), Zhimin Hu(胡智民), Dalong Guo(郭大龙), Junwen Gao(高俊文), Bennaceur Najjari, Shenyue Xu(许慎跃), Shuncheng Yan(闫顺成), Ke Yao(姚科), Ruitian Zhang(张瑞田), Yong Gao(高永), and Xiaolong Zhu(朱小龙)
Chin. Phys. B, 2022, 31 (**9**): 093401. DOI: 10.1088/1674-1056/ac8736

The influence of collision energy on magnetically tuned ^{6}Li-^{6}Li Feshbach resonance

Rong Zhang(张蓉), Yong-Chang Han(韩永昌), Shu-Lin Cong(丛书林), and Maksim B Shundalau
Chin. Phys. B, 2022, 31 (**6**): 063402. DOI: 10.1088/1674-1056/ac4cc3

Enhancement of electron-ion recombination rates at low energy range in the heavy ion storage ring CSRm

Nadir Khan, Zhong-Kui Huang(黄忠魁), Wei-Qiang Wen(汶伟强), Shu-Xing Wang(汪书兴), Han-Bing Wang(汪寒冰), Wan-Lu Ma(马万路), Xiao-Long Zhu(朱小龙), Dong-Mei Zhao(赵冬梅), Li-Jun Mao(冒立军), Jie Li(李杰), Xiao-Ming Ma(马晓明), Mei-Tang Tang(汤梅堂), Da-Yu Yin(殷达钰), Wei-Qing Yang(杨维青), Jian-Cheng Yang(杨建成), You-Jin Yuan(原有进), Lin-Fan Zhu(朱林繁), Xin-Wen Ma(马新文)
Chin. Phys. B, 2020, 29 (**3**): 033401. DOI: 10.1088/1674-1056/ab69eb

---

Theoretical study of electron-ion resonant recombination of Be-like Si^{10+} ion

Jing-Lin Rui(芮静琳)[1,2], Jian-Ping Pan(潘建平)[2,3], Lu-You Xie(颉录有)[2,†], Yu-Long Ma(马玉龙)[2], and Chen-Zhong Dong(董晨钟)[2,‡]

[1] *School of Cyber Security, Gansu University of Political Science and Law, Lanzhou* 730070, *China*
[2] *Key Laboratory of Atomic and Molecular Physics and Functional Materials of Gansu Province, College of Physics and Electronic Engineering, Northwest Normal University, Lanzhou* 730070, *China*
[3] *Guazhou County No.* 1 *Middle School, Guazhou* 736100, *China*

(Received 26 September 2025; revised manuscript received 18 December 2025; accepted manuscript online 19 December 2025)

Theoretical investigations of L-shell $\Delta n = 1$ ($2s \rightarrow 3l$) and 2 ($2s \rightarrow 4l$) as well as K-shell $\Delta n = 1$ ($1s \rightarrow 2l$) electron-ion resonant recombination for both the ground state ($2s^2\ ^1S_0$) and the long-lived metastable state ($2s2p\ ^3P_0$) of Be-like Si^{10+} are performed. The calculations include not only the dominant dielectronic recombination (DR), but also high-order trielectronic (TR) and quadruelectronic recombination (QR) processes. Level-by-level calculations are performed for resonance energies and resonance strengths using the relativistic configuration interaction method. The theoretical rate coefficients are presented and compared with the experimental results measured at the heavy-ion storage ring TSR. When considering fractional populations of 93% and 7% for the ground state $2s^2\ ^1S_0$ and the metastable state $2s2p\ ^3P_0$, the present rate coefficients agree well with the experimental measurements. The contributions of TR are important, which is about 9.26% to the total rate coefficient of L-shell recombination. The plasma rate coefficients are also calculated, and an analytical formula is presented for convenient modeling of astrophysical and fusion plasmas.

Keywords: dielectronic recombination, rate coefficient, metastable states, silicon

PACS: 34.80.Lx, 36.20.Kd, 95.30.Dr, 31.15.ve

DOI: 10.1088/1674-1056/ae2f54 **CSTR:** 32038.14.CPB.ae2f54

1. Introduction

Resonant recombination processes are important electron-ion collision processes in photoionized and collisionally ionized plasmas.[1–4] These processes include dielectronic recombination (DR), high-order trielectronic recombination (TR),[5,6] and quadruelectronic recombination (QR).[6–8] Since resonant recombination changes the charge state of ions, it significantly influences charge distribution, level population, and radiative spectra in most plasmas.[9,10]

In DR, an electron is captured resonantly from the continuum into highly charged ions while exciting a bound electron, forming an intermediate doubly excited state. Subsequently, the intermediate doubly excited state undergoes radiative decay, stabilizing into energetically lower states.[9,11] When considering electron correlation effects, higher-order resonant recombination including TR and QR may also occur.[3] The difference is that TR and QR involve the simultaneous excitation of two or even three bound electrons.[4] TR was first observed in the recombination spectrum of Be-like Cl^{13+} ions at the TSR heavy-ion storage ring,[5] and found it contributes to the total recombination rate up to 20%–40% for plasmas with temperatures ranging from 1 eV to 100 eV. Since then, many theoretical and experimental efforts have been made to investigate TR for Be-like ions.[2,12–18] These studies mainly focus on the resonances associated with L-shell $\Delta n = 0$ ($2s \rightarrow 2p$) transitions. Beilmann *et al.*[6,7,19] expanded the measurements of TR and QR to K-shell $\Delta n = 1$ ($1s \rightarrow 2l$) transitions for the Ar, Fe, and Kr ions at Heidelberg electron beam ion trap (EBIT), and found that the resonance strengths of higher-order processes become stronger as the atomic number Z decreases.[6] Shah *et al.*[4,20,21] measured the x-ray emission asymmetries in the K-shell recombination of Fe^{24+} to Fe^{18+}, and Kr^{30+} ions at the FLASH-EBIT, and proved that TR and QR play an important role in x-ray polarization.[4]

Silicon is an abundant astrophysical element. Its emission and absorption spectral lines have been extensively detected across various astronomical environments.[22–27] Interpreting and analyzing these spectral lines require precise atomic parameters for silicon. In recent years, Gu[28] calculated the rate coefficients for L- and K-shell DR of H- to Ne-like isosequences, including Si^{4+}–Si^{13+}. Colgan *et al.*[29] calculated the rate coefficients associated with L-shell resonant recombination of Be-like isoelectronic sequence including Si^{10+}, using AUTOSTRUCTURE. Orban *et al.*[14] measured the L-shell recombination rate coefficients of Si^{10+} across electron energies ranging from 0 to 43 eV at the CRYRING electron cooler. In

†Corresponding author. E-mail: xiely@nwnu.edu.cn
‡Corresponding author. E-mail: dongcz@nwnu.edu.cn

© 2026 Chinese Physical Society and IOP Publishing Ltd. All rights, including for text and data mining, AI training, and similar technologies, are reserved.

2016, Bernhardt *et al.*[30] extended the previous measurement of Orban *et al.*[14] to a much wider collision energies up to 2000 eV, at the TSR heavy-ion storage ring. The new measurements reveal high-energy L- and K-shell resonances that have not been reported before.

The Si^{10+} ion has the ground state $2s^2\ {}^1S_0$, and its metastable state $2s2p\ {}^3P_0$ has long lifetime with $t = 16.64$ s,[30,31] which might exist in the ion beams used for recombination experiments.[1,15,30] In this work, we focus on theoretical investigations of resonant recombination for Si^{10+} in both the initial ground state and the metastable state, for the L-shell $\Delta n = 1$ and 2, as well as the K-shell $\Delta n = 1$ processes. Level-by-level calculations for resonance energies, resonance strengths, and rate coefficients are carried out utilizing the flexible atomic code (FAC).[32] Based on these calculations, the experimental spectra reported by Bernhardt *et al.*[30] are modeled and identified. This paper is structured as follows. In the subsequent section, the theoretical method is presented. In Section 3, the theoretical recombination rate coefficients for Si^{10+} are presented and discussed. Finally, a conclusion is given in Section 4.

2. Theoretical methods

The electron-ion resonant recombination can be formulated as

$$A^{q+}(i) + \varepsilon\, e^- \rightarrow [A^{(q-1)+}]^{**}(d) \rightarrow [A^{(q-1)+}]^{*}(f) + h\nu. \quad (1)$$

Here, $A^{q+}(i)$ denotes the ion in its initial state (i). $[A^{(q-1)+}]^{**}(d)$ is the resulting unstable intermediate excited state (d). $[A^{(q-1)+}]^{*}(f)$ is the radiative decay finial state (f) of the recombined ion.

In isolated resonance approximation,[33] the resonance strength for a particular intermediate excited state (d) can be expressed as[9]

$$S_d = \frac{g_d \pi^2}{2 g_i E_d} A^{\mathrm{a}}(d \rightarrow i) B(d). \quad (2)$$

In the above expression, the resonant capture rate is described by its time-reversed autoionization rate $A^{\mathrm{a}}(d \rightarrow i)$. The g_i and g_d are the statistical weights of the initial state i and intermediate state d. E_d denotes the resonance energy. $B(d)$ is the radiative branching ratio[11]

$$B(d) = \frac{\sum_f A^{\mathrm{r}}(d \rightarrow f)}{\sum_{i'} A^{\mathrm{a}}(d \rightarrow i') + \sum_{f'} A^{\mathrm{r}}(d \rightarrow f')}, \quad (3)$$

where $A^{\mathrm{r}}(d \rightarrow f)$ represents the radiative decay rates from the state d to radiative decay finial state f. $\sum_{i'} A^{\mathrm{a}}(d \rightarrow i') + \sum_{f'} A^{\mathrm{r}}(d \rightarrow f')$ takes the sum over all the individual autoionization and radiative rates of state d. The radiative decay rate A^{r} is expressed as[11]

$$A^{\mathrm{r}}(d \rightarrow f') = \frac{4\omega_{\mathrm{p}}^3}{3c^3 g_d} |\langle \psi_{f'} | T^{(t)} | \psi_d \rangle|^2 \quad (4)$$

here ψ_d and $\psi_{f'}$ denote the atomic state functions for the intermediate and final states of the recombination system. $T^{(t)}$ represents the multipole radiative tensor operator, here only the electronic dipole allowed (E1) transition is considered. c is the velocity of light, while ω_{p} denotes the frequency of the photons emitted during decay.

The autoionization rate $A^{\mathrm{a}}(d \rightarrow i')$ from the intermediate state d to autoionization final state (initial charge state) i can be expressed as[11]

$$A^{\mathrm{a}}(d \rightarrow i') = 2 \sum_{\kappa} |\langle \psi_{i'}, \kappa; J_{\mathrm{T}} M_{\mathrm{T}} | \sum_{p<q} (V_{\mathrm{Coul}} + V_{\mathrm{Breit}}) | \psi_d \rangle|^2, \quad (5)$$

similarly, $\psi_{i'}$ are the atomic state functions of the state i', κ is the relativistic angular quantum number,[11] $|\psi_{i'}, \kappa; J_{\mathrm{T}} M_{\mathrm{T}}\rangle$ is the coupling wavefunction,[11] with total angular momentum J_{T} and z component M_{T}. Besides the Coulomb operator $V_{\mathrm{Coul}} = 1/r_{pq}$,[34] the Breit operator V_{Breit} given in the zero-frequency limit is also incorporated[35,36]

$$V_{\mathrm{Breit}} = -\sum_{p<q}^{N} \frac{1}{2 r_{pq}} \left[\boldsymbol{\alpha}_p \cdot \boldsymbol{\alpha}_q + \frac{(\boldsymbol{\alpha}_p \cdot \boldsymbol{r}_{pq})(\boldsymbol{\alpha}_q \cdot \boldsymbol{r}_{pq})}{r_{pq}^2} \right], \quad (6)$$

where α_p and α_q are the Dirac matrices.

The resonant recombination cross section can be well approximated by a Lorentzian line-shape $L(\varepsilon_{\mathrm{e}}) = \frac{\Gamma/2\pi}{(E_d - \varepsilon_{\mathrm{e}})^2 + \Gamma^2/4}$ and the resonance strength S_d by[9]

$$\sigma(\varepsilon_{\mathrm{e}}) = S_d L_d(\varepsilon_{\mathrm{e}}). \quad (7)$$

For comparison with experimental rate coefficients, the calculated cross section has to be convoluted with the relevant electron velocity distribution[37]

$$\alpha(\varepsilon) = \int \sigma(v) v f(v) \mathrm{d}^3 v, \quad (8)$$

where $f(v)$ is the velocity distribution of the electron beam. For electron–ion merged beam experiments conducted at storage rings, a Maxwell distribution[15,38] with longitudinal and transverse temperatures $T_{\parallel}$ and $T_{\perp}$ is employed[39]

$$f(v) = \left(\frac{m_{\mathrm{e}}}{2\pi k T_{\parallel}}\right)^{\frac{1}{2}} \exp\left[-\frac{m_{\mathrm{e}}\left(v_{\parallel} - v_0\right)^2}{2kT_{\parallel}}\right] \times \frac{m_{\mathrm{e}}}{2\pi k T_{\perp}} \exp\left(-\frac{m_{\mathrm{e}} {v_{\perp}}^2}{2kT_{\perp}}\right), \quad (9)$$

where k stands for the Boltzmann constant, and m_{e} denotes the electron mass. $v_{\parallel}$ and $v_{\perp}$ represent the longitudinal and transverse components of the electron velocity, respectively. The detuning velocity $v_0 = \sqrt{2\varepsilon/m_{\mathrm{e}}}$ defines the relative energy.[39] Ultimately, the recombination rate coefficient can be calculated as follows:

$$\alpha(\varepsilon) = \frac{S_d v_d}{m_{\mathrm{e}} \sigma_{\perp}^2 \zeta} \exp\left(-\frac{v_d^2 - v_0^2 \zeta^{-2}}{\sigma_{\perp}^2}\right)$$

$$\times\left[\mathrm{erf}\left(\frac{v_0+v_d\zeta^2}{\sigma_\parallel\zeta}\right)-\mathrm{erf}\left(\frac{v_0-v_d\zeta^2}{\sigma_\parallel\zeta}\right)\right], \quad (10)$$

where v_d denotes the relative velocity corresponding to the resonance energy E_d, and $\sigma_{\parallel,\perp}=\left(2kT_{\parallel,\perp}/m_\mathrm{e}\right)^{1/2}$, $\zeta=\left(1-T_\parallel/T_\perp\right)^{1/2}$.[10]

In astrophysical and fusion plasmas, electrons exhibit a broader Maxwellian–Boltzmann velocity distribution characterized by the electron temperature T_e

$$f(v,T_\mathrm{e})=\left(\frac{m_\mathrm{e}}{2\pi kT_\mathrm{e}}\right)^{3/2}\exp\left(-\frac{m_\mathrm{e}v^2}{2kT_\mathrm{e}}\right). \quad (11)$$

The plasma rate coefficient is temperature-dependent, which can be expressed as follows:[40]

$$\alpha(T_\mathrm{e})=\frac{4E_d}{\left(2\pi m_\mathrm{e}k^3T_\mathrm{e}^3\right)^{1/2}}\exp\left(-\frac{E_d}{kT_\mathrm{e}}\right)S_d. \quad (12)$$

3. Result and discussion

The L-shell resonant recombination associated with $\Delta n=1$ and 2 transitions of Si^{10+} in ground state $2s^2\ {}^1S_0$ can be written as (the core electrons $1s^2$ are omitted)

$$\varepsilon\,e^-+Si^{10+}(2s^2\ {}^1S_0)\rightarrow\begin{cases}\left[Si^{9+}(2s3lnl')\right]^{**}\\ \left[Si^{9+}(2p3lnl')\right]^{***}\\ \left[Si^{9+}(2s4lnl')\right]^{**}\\ \left[Si^{9+}(2p4lnl')\right]^{***}\end{cases}\quad\begin{array}{ll}\Delta n=1 & \mathrm{DR},\ \ (a)\\ \Delta n=1 & \mathrm{TR},\ \ (b)\\ \Delta n=2 & \mathrm{DR},\ \ (c)\\ \Delta n=2 & \mathrm{TR},\ \ (d)\end{array}\rightarrow\left[Si^{9+}\left(2lnl'\right)\right]^*+h\nu. \quad (13)$$

Here Eqs. (13(a)) and (13(b)) denote the $\Delta n=1$ DR ($2s\rightarrow 3l$) and TR ($2s^2\rightarrow 2p+3l$) processes, which form the intermediate doubly excited states $[Si^{9+}(2s3lnl')]^{**}$ and triply excited states $[Si^{9+}(2p3lnl')]^{***}$, respectively. Equations (13(c)) and (13(d)) denote the $\Delta n=2$ DR ($2s\rightarrow 4l$) and TR ($2s^2\rightarrow 2p+4l$) processes. Here, nl' is the captured (Rydberg) electron. All the excited states with $3\le n\le 25, 0\le l'\le 15$ are included.

The K-shell $\Delta n=1$ resonant recombination for Si^{10+} can be described as follows:

$$\varepsilon\,e^-+Si^{10+}(1s^22s^2\ {}^1S_0)\rightarrow\begin{cases}\left[Si^{9+}\left(1s2s^22pnl'\right)\right]^{**}\\ \left[Si^{9+}\left(1s2s2p^2nl'\right)\right]^{***}\\ \left[Si^{9+}\left(1s2p^3nl'\right)\right]^{****}\end{cases}\quad\begin{array}{ll}\mathrm{DR}, & (a)\\ \mathrm{TR}, & (b)\\ \mathrm{QR}, & (c)\end{array}\rightarrow\left[Si^{9+}\left(1s^22l^2nl'\right)\right]^*+h\nu. \quad (14)$$

Here Eqs. (14(a))–(14(c)) denote the DR ($1s\rightarrow 2p$), TR ($1s+2s\rightarrow 2p^2$), and QR ($1s+2s^2\rightarrow 2p^3$) processes, respectively. $[Si^{9+}(1s2p^3nl')]^{****}$ is the quadruply excited states associated with QR. The states with $2\le n\le 25$ and $0\le l'\le 15$ are included in our calculation.

The resonant recombination of Si^{10+} ion in the initial metastable state $2s2p\ {}^3P_0$ resembles that of the ground state. For the sake of conciseness, we omitted details.

Using FAC code,[32] we calculated the energy level and wave function for L- and K-shell resonant recombination of Si^{10+}. Strong configuration mixings among the DR, TR, and QR resonance states are considered. The Breit interaction in the zero-frequency limit and quantum electrodynamics (QED) corrections are fully considered.

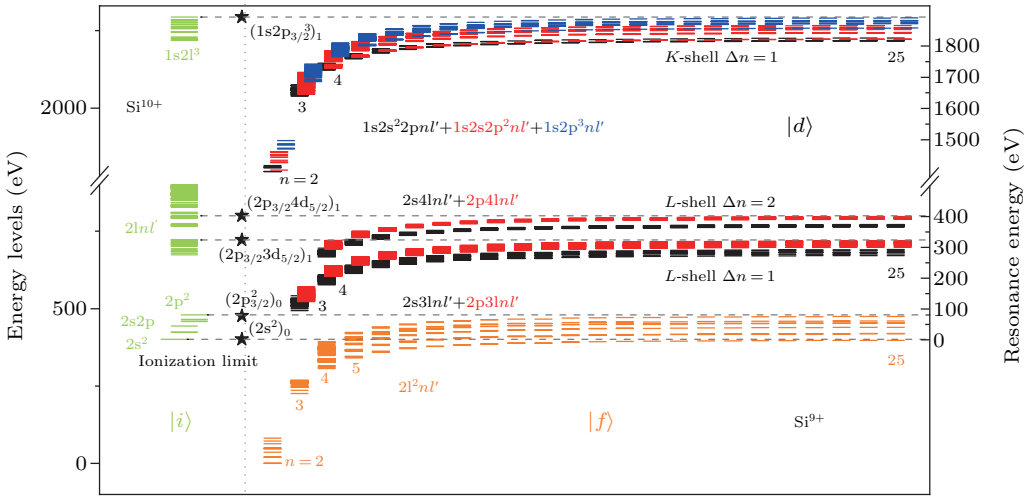


Fig. 1. The energy level diagram for Be-like Si^{10+} (left), and B-like Si^{9+} (right) formed by L- and K-shell resonant recombination in the ground state. The colored horizontal bars show the autoionization final states $|i\rangle$ (green); doubly (black), triply (red), and quadruply (blue) excited states $|d\rangle$ in DR, TR, and QR processes; as well as the radiation final states $|f\rangle$ (orange) of the Si^{10+} ions. The horizontal dashed line indicates the calculated ionization limit for Si^{10+} ions (see Table 1), which exhibits good agreement with the NIST[41] (star).

3.1. Energy level

To obtain accurate energy levels, especially for the resonance states involved, we carried out a relativistic configuration interaction (CI) calculation for Si^{10+}, and formed Si^{9+} ions. The resonance states (including DR, TR, and QR) and radiative decay final states involved in the present work are given in Eqs. (13) and (14). Four CI models, labeled CI($n = 10$), CI($n = 15$), CI($n = 20$), and CI($n = 25$), were considered to check the convergence of calculated energy levels for Si^{9+} ions. These models gradually expand the CI calculation with including more higher (n double, triple) excited states and more radiative final states. It is found that excellent convergence of the calculations is achieved when n is increased to 25 for Si^{9+}. Compared to the energy obtained with n increased to 20, when n is increased to 25, the energy shows slight changes with the difference less than 0.0003 eV and 0.004 eV for L-shell and K-shell transitions, respectively. Table 1 presents the calculated energies of Si^{9+} (labeled 1–49), along with the first ionization limit $2s^2$ and the highest energy level of the configurations $2l^2$, 2p3l, 2p4l, and $1s2l^3$ of Si^{10+} (labeled 50–54). For comparison, the values from the NIST[41] are also tabulated. The calculated results are in good agreement with the NIST values, with deviations less than 1.82%.

Figure 1 presents the energy levels diagram for Be-like Si^{10+} (left), and B-like Si^{9+} (right) formed by L- and K-shell resonant recombination in the ground state. The black, red, and blue horizontal bars represent the doubly, triply, and quadruply excited states associated with DR, TR, and QR processes of Si^{10+}, respectively. In the resonance energy range of E_d = 92.96 eV–317.87 eV, the $2s3lnl'$ (DR) and $2p3lnl'$ (TR) (n = 3–25) excited states contribute to the L-shell $\Delta n = 1$ process. Above the resonance energy of 266 eV, the L-shell $\Delta n = 2$ process will occur, and form the $2s4lnl'$ (DR) and $2p4lnl'$ (TR) (n = 3–25) excited states. When the resonance energy exceeds 1398 eV, the K-shell resonant recombination will take place, and form the $1s2s^22pnl'$ (DR), $1s2s2p^2nl'$ (TR), and $1s2p^3nl'$ (QR) (n = 2–25) excited states.

3.2. The L-shell rate coefficients

We calculated the resonant recombination rate coefficients for both the ground state $2s^2\ {}^1S_0$ (Fig. 2) and the metastable state $2s2p\ {}^3P_0$ (Fig. 3) of Si^{10+} ion. In the calculation, three CI models, labeled CI($n = 10$), CI($n = 15$), and CI($n = 25$), have been considered. When the CI calculation is further extended to the CI($n = 25$) model incorporating more resonant excited states and radiative final states up to n_{max} = 25, more resonance peaks appear in the high - energy region, and the calculated results show better agreement with the experiment. Thus, our theoretical results are presented by employing the model CI($n = 25$) ($n_{max} = 25$).

Table 1. The calculated energy levels (in eV) of Si^{9+}, as well as the first ionization limit $2s^2$ and the highest level of the configurations $2l^2$, 2p3l, 2p4l, and $1s2l^3$ of Si^{10+} ions, together with the NIST values.[41]

Ions	Label	State	Energies (eV)		
			This	NIST[41]	Diff.
Si^{9+}	1	$(2s^22p_{1/2})_{1/2}$	0	0	0
	2	$(2s^22p_{3/2})_{3/2}$	0.86	0.87	−0.86%
	3	$(2s2p^2_{1/2})_{1/2}$	19.61	19.96	−1.74%
	4	$(2s2p_{1/2}2p_{3/2})_{3/2}$	19.92	20.27	−1.74%
	5	$(2s2p^2_{3/2})_{5/2}$	20.36	20.71	−1.71%
	6	$(2s2p_{1/2}2p_{3/2})_{5/2}$	36.17	35.69	1.34%
	7	$(2s2p_{1/2}2p_{3/2})_{3/2}$	36.17	35.69	1.34%
	8	$(2s2p^2_{3/2})_{1/2}$	46.22	45.59	1.39%
	9	$(2s2p_{1/2}2p_{3/2})_{1/2}$	49.24	48.36	1.82%
	10	$(2s2p^2_{3/2})_{3/2}$	49.73	48.85	1.81%
	11	$(2p_{1/2}2p^2_{3/2})_{3/2}$	63.21	63.15	0.10%
	12	$(2p_{1/2}2p^2_{3/2})_{5/2}$	72.13	71.35	1.10%
	13	$(2p_{1/2}2p^2_{3/2})_{3/2}$	72.13	71.34	1.11%
	14	$(2p_{1/2}2p^2_{3/2})_{1/2}$	81.25	80.19	1.32%
	15	$(2p^3_{3/2})_{3/2}$	81.33	80.27	1.31%
	16	$(2s^23d_{3/2})_{3/2}$	244.84	245.40	−0.23%
	17	$(2s^23d_{5/2})_{5/2}$	244.90	245.46	−0.23%
	18	$(2s2p_{1/2}3s)_{1/2}$	246.13	247.08	−0.38%
	19	$(2s2p_{1/2}3s)_{3/2}$	246.41	247.37	−0.39%
	20	$(2s2p^3_{3/2}3s)_{5/2}$	246.93	247.92	−0.40%
	21	$(2s2p_{1/2}3s)_{1/2}$	251.04	251.82	−0.31%
	22	$(2s2p^3_{3/2}3s)_{3/2}$	251.62	252.41	−0.31%
	23	$(2s2p_{1/2}3p_{1/2})_{1/2}$	255.72	255.98	−0.10%
	24	$(2s2p_{1/2}3p_{1/2})_{3/2}$	255.84	256.24	−0.15%
	25	$(2s2p_{1/2}3p_{3/2})_{3/2}$	260.46	261.08	−0.24%
	26	$(2s2p_{3/2}3p_{3/2})_{5/2}$	261.01	261.64	−0.21%
	27	$(2s2p_{3/2}3p_{3/2})_{1/2}$	263.86	264.41	−0.21%
	28	$(2s2p_{1/2}3d_{3/2})_{1/2}$	265.91	266.68	−0.29%
	29	$(2s2p_{1/2}3d_{5/2})_{3/2}$	265.97	266.68	−0.27%
	30	$(2s2p_{1/2}3d_{5/2})_{5/2}$	266.07	266.74	−0.25%
	31	$(2s2p_{3/2}3d_{5/2})_{7/2}$	266.29	267.04	−0.28%
	32	$(2s2p_{3/2}3d_{5/2})_{3/2}$	266.46	267.02	−0.21%
	33	$(2s2p_{3/2}3d_{3/2})_{5/2}$	266.54	267.12	−0.22%
	34	$(2s2p_{3/2}3d_{5/2})_{5/2}$	267.18	267.92	−0.27%
	35	$(2s2p_{3/2}3d_{3/2})_{3/2}$	267.33	268.07	−0.27%
	36	$(2s2p_{3/2}3s)_{3/2}$	267.49	267.60	−0.04%
	37	$(2s2p_{1/2}3d_{5/2})_{5/2}$	270.99	271.35	−0.13%
	38	$(2s2p_{3/2}3d_{3/2})_{7/2}$	271.52	271.92	−0.15%
	39	$(2s2p_{3/2}3d_{5/2})_{3/2}$	272.23	272.67	−0.16%
	40	$(2s2p_{3/2}3d_{5/2})_{1/2}$	272.54	272.99	−0.17%
	41	$(2s2p_{3/2}3p_{1/2})_{1/2}$	277.28	278.51	−0.44%
	42	$(2s2p_{3/2}3d_{5/2})_{7/2}$	285.45	285.15	0.11%
	43	$(2s2p_{3/2}3d_{3/2})_{5/2}$	285.48	285.15	0.11%
	44	$(2s2p_{3/2}3d_{3/2})_{3/2}$	286.74	286.47	0.09%
	45	$(2s2p_{3/2}3d_{5/2})_{5/2}$	286.82	286.58	0.08%
	46	$(2p_{1/2}2p_{3/2}3d_{5/2})_{5/2}$	302.96	303.07	−0.04%
	47	$(2p^2_{3/2}3d_{3/2})_{3/2}$	303.15	303.30	−0.05%
	48	$(2s^24d_{3/2})_{3/2}$	313.38	314.34	−0.31%
	49	$(2s^24d_{5/2})_{5/2}$	313.40	314.34	−0.30%
Si^{10+}	50	$(2s^2)_0$	400.25	401.38	−0.28%
	51	$(2p^2_{3/2})_0$	477.54	476.86	0.14%
	52	$(2p_{3/2}3d_{5/2})_1$	721.40	721.62	−0.07%
	53	$(2p_{3/2}4d_{5/2})_1$	799.68	799.95	−0.03%
	54	$(1s2p^3_{3/2})_1$	2294.61	2293.61	0.04%

Figure 2 illustrates the calculated rate coefficients associated with the L-shell $\Delta n = 1$ and 2 transitions of Si^{10+} in the ground state $2s^2\ ^1S_0$. For comparison, the cross sections have been convoluted with the experimental electron velocity distribution characterized by the temperatures of the electron beam $kT_{\parallel} = 0.093$ meV and $kT_{\perp} = 0.5$ eV[30] in longitudinal and transversal directions. The total (DR + TR) rate coefficients (black line) and the contributions of TR (red areas) are shown in Fig. 2(a). The TR process is important, contributing 8.67% to the total rate coefficients. Obviously, the $\Delta n = 1$ resonance forms $(2s/2p)3lnl'$ (DR/TR) resonance states located at the resonant energy regions of 87 eV to 320 eV, which can be divided into three partial channels including $213snl'$, $213pnl'$, and $213dnl'$ (see Figs. 2(b)–2(d)) according to $3l$ ($l = s, p, d$) values. Those resonant peaks are identified by the standard notations LMM, LMN, LMO, and LMP. Compared to the $\Delta n = 1$ resonance, the $\Delta n = 2$ resonance is rather weak, located at a higher resonance energy range of 261 eV to 399 eV, which are mainly from $(2s/2p)4lnl'$ (DR/TR) resonances state (see Fig. 2(e)).

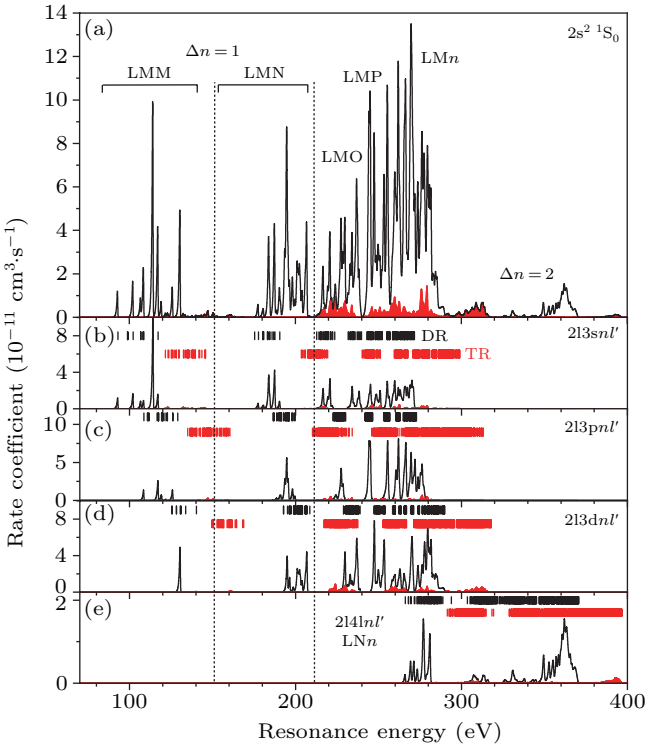


Fig. 2. The calculated resonant recombination rate coefficients of Si^{10+} associated with L-shell Δn = 1 and 2 transition in ground state $2s^2\ ^1S_0$. The black line represents the DR + TR rate coefficient, and the red areas denote the contributions of TR. (a) The total rate coefficient. (b)–(d) The contributions from $213snl'$, $213pnl'$, $213dnl'$ resonant channels of $\Delta n = 1$ transitions, respectively. (e) The contributions of $\Delta n = 2$ transitions. The black and red vertical bars show the DR and TR resonance positions.

Figure 3 presents the calculated total (DR + TR) rate coefficients (black line) (see Fig. 3(a)) for L-shell $\Delta n = 1$ and 2 resonant recombination of Si^{10+} in the metastable state $2s2p\ ^3P_0$. The contributions from the three resonant channels of $\Delta n = 1$, as well as the contribution of $\Delta n = 2$ process, are approximately 13.58%, 19.80%, 62.28%, and 4.34%, respectively. The resonance from the $213dnl'$ channel is the strongest. It is found that the TR contributes 13.35% to the total rate coefficients in the metastable state, which is larger than that in the ground state.

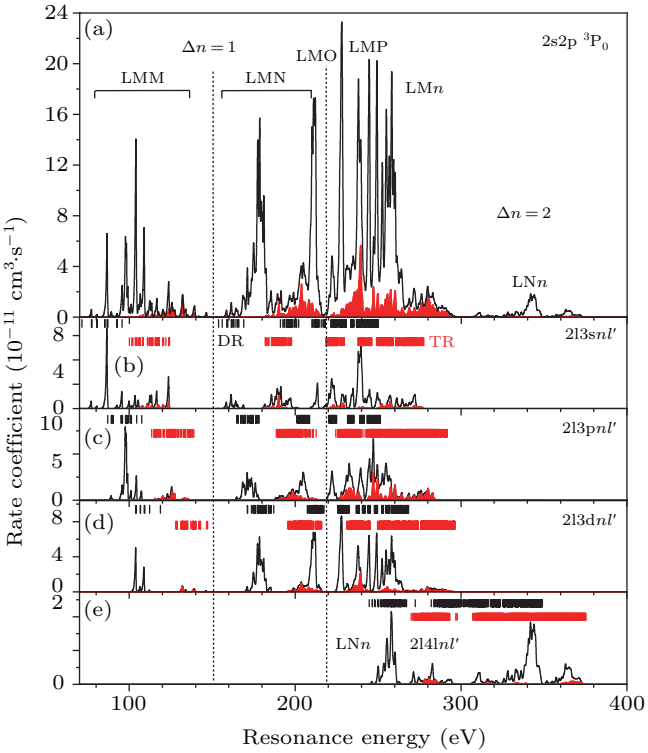


Fig. 3. Same as Fig. 2 but for the rate coefficients of Si^{10+} in the metastable state ($2s2p\ ^3P_0$).

In Table 2, the total recombination strength summed over $213snl'$, $213pnl'$, and $213dnl'$, and $214lnl'$ contributions for Si^{9+} ions in the ground states ($2s^2\ ^1S_0$) and the metastable state ($2s2p\ ^3P_0$) is listed. It is found that the most significant contribution originates from the $213dnl'$ channel, which is largely attributed to this channel's prominent resonant capture strength.

Table 2. Total resonant recombination strength (in cm^2·eV) summed all $213snl'$, $213pnl'$, and $213dnl'$, and $214lnl'$ contributions for Si^{9+} ions in the ground states ($2s^2\ ^1S_0$) and the metastable state ($2s2p\ ^3P_0$). ($A(B)$ denotes $A \times 10^B$)

Initial state	$213snl'$	$213pnl'$	$213dnl'$	$214lnl'$
$2s^2\ ^1S_0$	9.30(−19)	1.21(−18)	1.39(−18)	1.93(−19)
$2s2p\ ^3P_0$	9.56(−19)	1.39(−18)	4.38(−18)	3.05(−19)

In Fig. 4, the present rate coefficients for L-shell $\Delta n = 1$ and 2 resonant recombination of Si^{10+} are compared with the TSR experimental results by Bernhardt *et al.*[30] When considering that the initial Si^{10+} ion consists of 93% ground state ($2s^2\ ^1S_0$) and 7% metastable state ($2s2p\ ^3P_0$), the theoretical results show good agreement with the experimental measurements. In the figure, the blue lines show the contribution of the metastable state ($2s2p\ ^3P_0$) to the recombination spectrum. It can be seen that in the resonance energy ranges from 66.428 eV to 377.204 eV, the metastable state

$2s2p\ ^3P_0$ reveals a significant contribution to *L*-shell resonant recombination of Si^{10+} ions. Except for the LMM peak, the other peaks are mixed together. In Fig. 5, the LMM resonance peak is identified in detail. The resonance peak encompasses multiple individual resonances, with their resonance energies and resonance strengths listed in Table 3. Most of the strong peaks originate from the ground state, however, the peaks labeled *a*, *c*, and *e* could be entirely attributed to the $2s2p\ ^3P_0$ state. The strongest peaks (labeled *g*) are mainly from resonance $((2s3s)_0 3d_{5/2})_{3/2,5/2}$ with $E_d = 114.19$ eV, $S_d = 5.28 \times 10^{-20}$ cm^2·eV, and $E_d = 114.24$ eV, $S_d = 7.74 \times 10^{-20}$ cm^2·eV, respectively. In Table 4, we analyze and identify the *LMN* resonance peak, only the resonance states with $S_d > 5 \times 10^{-21}$ cm^2·eV are tabulated.

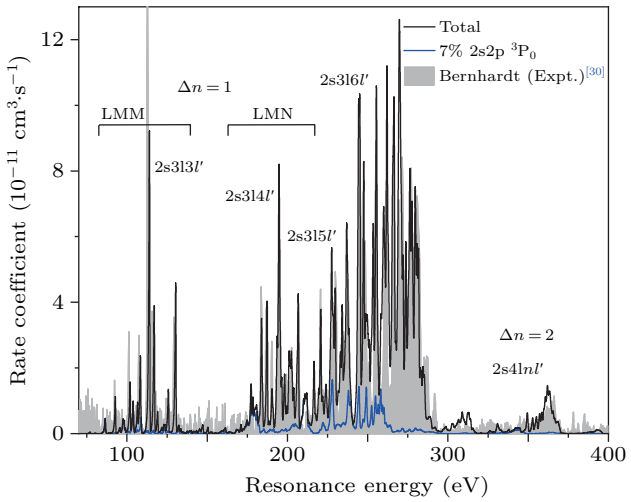


Fig. 4. Comparison of the calculated resonant recombination rate coefficients (black line) for *L*-shell $\Delta n = 1$ and 2 transitions of Si^{10+}, with the TSR measurements (gray area).[30] The ion beam composition of 93% ground state $2s^2\ ^1S_0$ +7% metastable state ($2s2p\ ^3P_0$) is considered. The blue line shows the contribution from the metastable state.

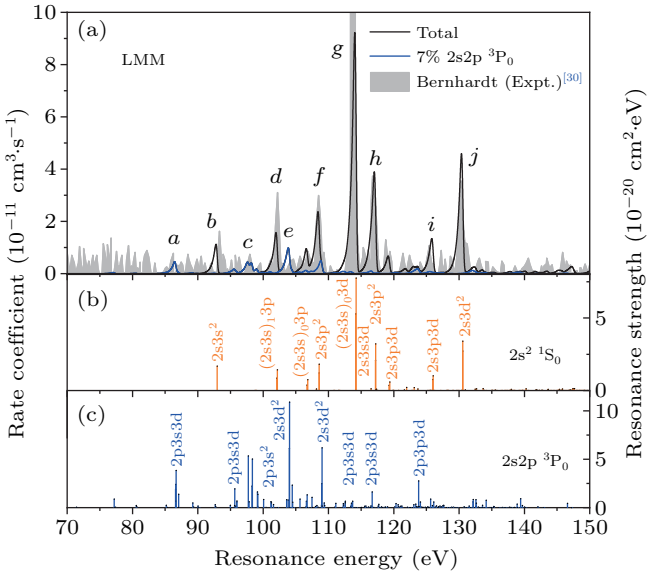


Fig. 5. The LMM resonant recombination rate coefficients and resonance strengths of Si^{10+} ion. (a) Comparison of the calculated rate coefficients (black line) with the TSR measurements (gray area).[30] (b) and (c) The resonance strengths from the state $2s^2\ ^1S_0$ (orange line) and $2s2p\ ^3P_0$ (blue line). The dominant resonances are also listed in Table 2.

Table 3. Calculated resonance energies E_d (in eV) and resonance strengths (in cm^2·eV) for Si^{10+} ions in the LMM resonant recombination process. Only the resonance states with $S_d > 5 \times 10^{-21}$ (cm^2·eV) are tabulated. ($A(B)$ denotes $A \times 10^B$).

Peaks	Resonance state	Initial state	Type	Resonance energy	Resonance strength
a	$((2s3s)_1 3d_{3/2})_{1/2}$	$2s2p\ ^3P_0$	DR	86.59	1.90(−20)
	$((2s3s)_1 3d_{3/2})_{3/2}$	$2s2p\ ^3P_0$	DR	86.61	2.39(−20)
	$((2s3s)_1 3d_{3/2})_{5/2}$	$2s2p\ ^3P_0$	DR	86.63	6.82(−21)
	$((2s3s)_1 3d_{5/2})_{7/2}$	$2s2p\ ^3P_0$	DR	86.67	3.85(−20)
	$((2s3s)_1 3d_{5/2})_{3/2}$	$2s2p\ ^3P_0$	DR	87.05	1.37(−20)
b	$(2s3s^2)_{1/2}$	$2s^2\ ^1S_0$	DR	92.96	1.68(−20)
c	$((2s3s)_1 3d_{5/2})_{3/2}$	$2s2p\ ^3P_0$	DR	95.66	1.94(−20)
	$((2s3p_{3/2})_1 3d_{5/2})_{5/2}$	$2s2p\ ^3P_0$	DR	95.97	5.78(−21)
	$((2s3p_{3/2})_1 3d_{3/2})_{3/2}$	$2s2p\ ^3P_0$	DR	95.97	6.80(−21)
	$((2s3p_{3/2})_1 3d_{3/2})_{5/2}$	$2s2p\ ^3P_0$	DR	97.73	5.33(−20)
	$((2s3p_{3/2})_1 3d_{5/2})_{7/2}$	$2s2p\ ^3P_0$	DR	97.85	6.07(−21)
	$((2s3p_{3/2})_2 3d_{3/2})_{3/2}$	$2s2p\ ^3P_0$	DR	98.31	2.22(−20)
	$((2s3p_{3/2})_2 3d_{3/2})_{5/2}$	$2s2p\ ^3P_0$	DR	98.37	5.02(−20)
	$((2s3p_{3/2})_2 3d_{5/2})_{5/2}$	$2s2p\ ^3P_0$	DR	99.14	1.63(−20)
	$((2s3p_{3/2})_2 3d_{3/2})_{1/2}$	$2s2p\ ^3P_0$	DR	99.18	1.37(−20)
d	$(2p_{1/2})_{1/2} 3s^2)_{1/2}$	$2s2p\ ^3P_0$	DR	100.07	8.37(−21)
	$((2s3p_{1/2})_1 3d_{5/2})_{3/2}$	$2s2p\ ^3P_0$	DR	101.19	6.12(−21)
	$((2s3p_{3/2})_2 3d_{5/2})_{5/2}$	$2s2p\ ^3P_0$	DR	101.25	5.01(−21)
	$((2s3s)_1 3p_{3/2})_{1/2}$	$2s^2\ ^1S_0$	DR	102.10	8.53(−21)
	$((2s3s)_1 3p_{3/2})_{3/2}$	$2s^2\ ^1S_0$	DR	102.18	1.43(−20)
e	$((2p_{1/2}3s)_0 3p_{1/2})_{1/2}$	$2s2p\ ^3P_0$	DR	103.60	8.13(−21)
	$((2p_{1/2}3s)_1 3p_{1/2})_{3/2}$	$2s2p\ ^3P_0$	DR	103.83	7.78(−21)
	$((2s3d_{3/2})_1 3d_{5/2})_{5/2}$	$2s2p\ ^3P_0$	DR	104.01	6.11(−20)
	$((2s3d_{3/2})_2 3d_{5/2})_{7/2}$	$2s2p\ ^3P_0$	DR	104.05	1.09(−19)
	$((2s3p_{1/2})_0 3d_{5/2})_{5/2}$	$2s2p\ ^3P_0$	DR	104.45	2.31(−20)
	$((2s3p_{3/2})_2 3d_{3/2})_{7/2}$	$2s2p\ ^3P_0$	DR	104.51	5.68(−21)
f	$((2p_{1/2}3s)_1 3p_{3/2})_{3/2}$	$2s2p\ ^3P_0$	DR	105.64	8.86(−21)
	$(2s3d^2_{3/2})_{1/2}$	$2s2p\ ^3P_0$	DR	106.62	6.53(−21)
	$((2s3s)_0 3p_{1/2})_{1/2}$	$2s^2\ ^1S_0$	DR	106.72	3.75(−21)
	$((2s3d_{3/2})_1 3d_{5/2})_{3/2}$	$2s2p\ ^3P_0$	DR	106.74	1.32(−20)
	$((2s3s)_0 3p_{3/2})_{3/2}$	$2s^2\ ^1S_0$	DR	106.84	7.45(−21)
	$((2s3p_{3/2})_2 3d_{5/2})_{3/2}$	$2s2p\ ^3P_0$	DR	107.49	1.06(−20)
	$((2s3s)_1 3d_{3/2})_{5/2}$	$2s^2\ ^1S_0$	DR	108.16	1.03(−21)
	$((2s3p_{1/2})_1 3p_{3/2})_{5/2}$	$2s^2\ ^1S_0$	DR	108.58	1.81(−20)
	$((2s3s)_1 3d_{5/2})_{3/2}$	$2s^2\ ^1S_0$	DR	108.58	1.21(−20)
	$(2s3d^2_{5/2})_{5/2}$	$2s2p\ ^3P_0$	DR	108.96	2.48(−20)
	$((2s3d_{3/2})_1 3d_{5/2})_{7/2}$	$2s2p\ ^3P_0$	DR	109.03	6.17(−20)
g	$((2p_{1/2}3s)_1 3d_{3/2})_{5/2}$	$2s2p\ ^3P_0$	DR	112.58	6.58(−21)
	$((2p_{1/2}3s)_0 3d_{5/2})_{5/2}$	$2s2p\ ^3P_0$	DR	113.70	6.69(−21)
	$((2s3s)_0 3d_{3/2})_{3/2}$	$2s^2\ ^1S_0$	DR	114.19	5.28(−20)
	$((2s3s)_0 3d_{5/2})_{5/2}$	$2s^2\ ^1S_0$	DR	114.24	7.74(−20)
h	$((2p_{1/2}3s)_0 3d_{5/2})_{5/2}$	$2s2p\ ^3P_0$	DR	116.71	1.63(−20)
	$((2s3s)_1 3d_{5/2})_{3/2}$	$2s^2\ ^1S_0$	DR	117.19	2.09(−20)
	$((2s3p_{1/2})_1 3p_{3/2})_{5/2}$	$2s^2\ ^1S_0$	DR	117.22	3.21(−20)
i	$(((2p_{3/2})_{3/2}3s)_1 3d_{5/2})_{3/2}$	$2s2p\ ^3P_0$	TR	124.07	5.89(−21)
	$(((2p_{1/2})_{1/2}3p_{1/2})_1 3d_{5/2})_{3/2}$	$2s2p\ ^3P_0$	DR	125.64	8.90(−21)
	$((2s3p_{1/2})_0 3d_{5/2})_{5/2}$	$2s^2\ ^1S_0$	DR	125.98	7.54(−21)
	$((2s3p_{3/2})_2 3d_{3/2})_{7/2}$	$2s^2\ ^1S_0$	DR	126.04	1.01(−20)
	$(((2p_{3/2})_{3/2}3p_{1/2})_2 3d_{3/2})_{5/2}$	$2s2p\ ^3P_0$	TR	126.13	5.76(−21)
j	$((2s3d_{3/2})_1 3d_{5/2})_{7/2}$	$2s^2\ ^1S_0$	DR	130.56	2.72(−20)
	$((2s3d_{3/2})_2 3d_{5/2})_{9/2}$	$2s^2\ ^1S_0$	DR	130.56	3.40(−20)

Table 4. Same to Table 3, but for LMN resonant recombination process.

Resonance state	Initial state	Type	Resonance energy	Resonance strength
$((2s3p_{3/2})_2 4d_{3/2})_{3/2}$	$2s2p\ ^3P_0$	DR	171.25	5.05(−21)
$((2s3p_{1/2})_0 4d_{5/2})_{5/2}$	$2s2p\ ^3P_0$	DR	171.29	1.31(−20)
$((2s3d_{5/2})_3 4s)_{7/2}$	$2s2p\ ^3P_0$	DR	171.33	1.28(−20)
$((2s3p_{1/2})_1 4f_{5/2})_{5/2}$	$2s2p\ ^3P_0$	DR	173.76	5.12(−21)
$((2s3p_{3/2})_2 4d_{5/2})_{5/2}$	$2s2p\ ^3P_0$	DR	173.77	5.88(−21)
$((2s3d_{3/2})_1 4p_{1/2})_{3/2}$	$2s2p\ ^3P_0$	DR	174.88	1.65(−20)
$((2s3d_{3/2})_1 4p_{3/2})_{5/2}$	$2s2p\ ^3P_0$	DR	174.92	1.31(−20)
$((2s3d_{5/2})_2 4s)_{3/2}$	$2s2p\ ^3P_0$	DR	175.15	7.61(−21)
$((2s3d_{3/2})_1 4p_{3/2})_{3/2}$	$2s2p\ ^3P_0$	DR	175.31	1.02(−20)
$((2s3d_{5/2})_3 4p_{1/2})_{5/2}$	$2s2p\ ^3P_0$	DR	175.35	2.31(−20)
$((2s3d_{3/2})_1 4p_{3/2})_{1/2}$	$2s2p\ ^3P_0$	DR	175.89	1.21(−20)
$((2s3d_{5/2})_3 4p_{1/2})_{5/2}$	$2s2p\ ^3P_0$	DR	175.92	6.78(−21)
$((2s3d_{3/2})_1 4p_{3/2})_{5/2}$	$2s2p\ ^3P_0$	DR	177.23	1.75(−20)
$((2s3d_{3/2})_1 4d_{3/2})_{5/2}$	$2s2p\ ^3P_0$	DR	177.44	4.66(−20)
$((2s3d_{3/2})_2 4d_{3/2})_{7/2}$	$2s2p\ ^3P_0$	DR	177.49	8.95(−21)
$((2s3d_{5/2})_3 4d_{3/2})_{7/2}$	$2s2p\ ^3P_0$	DR	177.54	3.27(−20)
$((2s3d_{5/2})_3 4d_{5/2})_{11/2}$	$2s2p\ ^3P_0$	DR	177.56	1.08(−20)
$((2s3s)_1 4s)_{1/2}$	$2s^2\ ^1S_0$	DR	177.63	6.87(−21)
$((2s3d_{5/2})_3 4d_{5/2})_{7/2}$	$2s2p\ ^3P_0$	DR	177.76	2.25(−20)
$((2s3d_{3/2})_1 4d_{5/2})_{5/2}$	$2s2p\ ^3P_0$	DR	178.67	2.29(−20)
$((2s3d_{3/2})_1 4f_{5/2})_{7/2}$	$2s2p\ ^3P_0$	DR	178.68	5.04(−20)
$((2s3d_{5/2})_3 4d_{3/2})_{7/2}$	$2s2p\ ^3P_0$	DR	178.70	3.97(−20)
$((2s3d_{3/2})_2 4f_{5/2})_{9/2}$	$2s2p\ ^3P_0$	DR	178.73	2.24(−20)
$((2s3d_{5/2})_3 4d_{3/2})_{3/2}$	$2s2p\ ^3P_0$	DR	179.21	6.64(−21)
$((2s3d_{3/2})_1 4f_{7/2})_{7/2}$	$2s2p\ ^3P_0$	DR	179.21	1.03(−20)
$((2s3d_{5/2})_3 4f_{5/2})_{9/2}$	$2s2p\ ^3P_0$	DR	179.23	1.47(−20)
$((2s3d_{5/2})_3 4f_{5/2})_{7/2}$	$2s2p\ ^3P_0$	DR	179.68	8.25(−21)
$((2s3d_{5/2})_3 4f_{7/2})_{9/2}$	$2s2p\ ^3P_0$	DR	179.69	3.53(−20)
$((2s3d_{5/2})_2 4p_{1/2})_{5/2}$	$2s2p\ ^3P_0$	DR	179.69	1.03(−20)
$((2s3d_{5/2})_3 4d_{3/2})_{3/2}$	$2s2p\ ^3P_0$	DR	180.15	1.17(−20)
$((2s3d_{5/2})_3 4d_{3/2})_{5/2}$	$2s2p\ ^3P_0$	DR	180.15	5.45(−21)
$((2s3d_{3/2})_2 4d_{3/2})_{5/2}$	$2s2p\ ^3P_0$	DR	180.17	1.43(−20)
$((2s3d_{3/2})_2 4d_{3/2})_{7/2}$	$2s2p\ ^3P_0$	DR	180.30	2.87(−20)
$((2s3d_{3/2})_2 4f_{5/2})_{9/2}$	$2s2p\ ^3P_0$	DR	181.03	2.55(−20)
$((2s3d_{3/2})_2 4f_{5/2})_{7/2}$	$2s2p\ ^3P_0$	DR	181.25	2.62(−20)
$((2s3d_{5/2})_3 4f_{5/2})_{9/2}$	$2s2p\ ^3P_0$	DR	181.28	3.96(−20)
$((2s3d_{5/2})_3 4f_{7/2})_{7/2}$	$2s2p\ ^3P_0$	DR	181.59	1.67(−20)
$((2s3d_{5/2})_3 4f_{5/2})_{5/2}$	$2s2p\ ^3P_0$	DR	181.93	6.94(−21)
$((2s3d_{5/2})_2 4d_{5/2})_{5/2}$	$2s2p\ ^3P_0$	DR	182.40	1.09(−20)
$((2s3d_{3/2})_1 4f_{7/2})_{5/2}$	$2s2p\ ^3P_0$	DR	182.58	7.51(−21)
$((2s3d_{5/2})_2 4d_{3/2})_{7/2}$	$2s2p\ ^3P_0$	DR	182.68	1.86(−20)
$((2s3s)_1 4d_{3/2})_{5/2}$	$2s^2\ ^1S_0$	DR	184.05	2.14(−20)
$((2s3s)_1 4d_{5/2})_{3/2}$	$2s^2\ ^1S_0$	DR	184.06	1.43(−20)
$((2s3d_{5/2})_2 4f_{7/2})_{7/2}$	$2s2p\ ^3P_0$	DR	184.59	6.46(−21)
$((2s3s)_0 4p_{1/2})_{1/2}$	$2s^2\ ^1S_0$	DR	184.62	5.48(−21)
$((2s3s)_0 4p_{3/2})_{3/2}$	$2s^2\ ^1S_0$	DR	184.69	1.10(−20)
$((2s3d_{5/2})_2 4f_{5/2})_{9/2}$	$2s2p\ ^3P_0$	DR	185.47	1.28(−20)
$((2p_{1/2}3s)_0 4p_{1/2})_{1/2}$	$2s2p\ ^3P_0$	DR	185.70	5.22(−21)
$((2p_{1/2}3s)_0 4p_{3/2})_{3/2}$	$2s2p\ ^3P_0$	DR	186.05	8.07(−21)
$((2s3s)_0 4d_{3/2})_{3/2}$	$2s^2\ ^1S_0$	DR	187.56	1.95(−20)
$((2s3s)_0 4d_{5/2})_{5/2}$	$2s^2\ ^1S_0$	DR	187.61	2.87(−20)
$((2p_{1/2}3s)_0 4d_{3/2})_{3/2}$	$2s2p\ ^3P_0$	DR	188.20	5.90(−21)
$((2s3p_{3/2})_1 4d_{3/2})_{5/2}$	$2s^2\ ^1S_0$	DR	194.81	2.27(−20)
$((2s3p_{3/2})_1 4d_{5/2})_{7/2}$	$2s^2\ ^1S_0$	DR	194.94	3.29(−20)
$((2s3d_{3/2})_2 4s)_{3/2}$	$2s^2\ ^1S_0$	DR	195.14	1.73(−20)
$((2s3d_{5/2})_3 4s)_{5/2}$	$2s^2\ ^1S_0$	DR	195.20	2.59(−20)
$((2s3p_{1/2})_1 4f_{5/2})_{7/2}$	$2s^2\ ^1S_0$	DR	195.67	1.08(−20)
$((2s3p_{1/2})_1 4f_{7/2})_{9/2}$	$2s^2\ ^1S_0$	DR	195.78	1.48(−20)

Table 4. Continued.

Resonance state	Initial state	Type	Resonance energy	Resonance strength
$((2s3d_{5/2})_2 4s)_{5/2}$	$2s^2\ ^1S_0$	DR	196.66	1.06(−20)
$((2s3d_{5/2})_2 4s)_{3/2}$	$2s^2\ ^1S_0$	DR	196.68	7.30(−21)
$((2s3p_{3/2})_1 4f_{5/2})_{7/2}$	$2s^2\ ^1S_0$	DR	198.40	7.39(−21)
$((2s3p_{3/2})_2 4f_{5/2})_{9/2}$	$2s^2\ ^1S_0$	DR	198.42	8.87(−21)
$((2p_{1/2}3d_{5/2})_2 4s)_{5/2}$	$2s2p\ ^3P_0$	DR	199.23	6.31(−21)
$((2s3d_{5/2})_3 4f_{5/2})_{7/2}$	$2s^2\ ^1S_0$	DR	201.22	5.43(−21)
$((2s3d_{3/2})_2 4p_{3/2})_{7/2}$	$2s^2\ ^1S_0$	DR	201.25	6.55(−21)
$((2s3d_{3/2})_2 4d_{3/2})_{7/2}$	$2s^2\ ^1S_0$	DR	201.83	7.07(−21)
$((2s3d_{5/2})_2 4d_{3/2})_{9/2}$	$2s^2\ ^1S_0$	DR	201.90	8.76(−21)
$((2s3d_{3/2})_2 4f_{5/2})_{9/2}$	$2s^2\ ^1S_0$	DR	202.56	8.25(−21)
$((2s3d_{5/2})_2 4f_{7/2})_{11/2}$	$2s^2\ ^1S_0$	DR	202.62	1.00(−20)
$((2s3d_{3/2})_2 4f_{7/2})_{5/2}$	$2s^2\ ^1S_0$	DR	203.09	6.74(−21)
$((2s3d_{5/2})_3 4f_{7/2})_{7/2}$	$2s^2\ ^1S_0$	DR	203.12	9.09(−21)
$((2p_{3/2}3d_{3/2})_1 4p_{1/2})_{3/2}$	$2s2p\ ^3P_0$	TR	203.97	8.66(−21)
$((2s3d_{3/2})_2 4d_{5/2})_{9/2}$	$2s^2\ ^1S_0$	DR	204.21	6.66(−21)
$((2s3d_{5/2})_2 4d_{3/2})_{7/2}$	$2s^2\ ^1S_0$	DR	204.21	5.32(−21)
$((2s3d_{5/2})_2 4f_{7/2})_{7/2}$	$2s^2\ ^1S_0$	DR	206.12	5.03(−21)
$((2p_{1/2}3d_{5/2})_2 4f_{7/2})_{11/2}$	$2s2p\ ^3P_0$	DR	206.69	7.17(−21)
$((2s3d_{3/2})_2 4f_{7/2})_{11/2}$	$2s^2\ ^1S_0$	DR	206.99	2.45(−20)
$((2s3d_{5/2})_2 4f_{5/2})_{9/2}$	$2s^2\ ^1S_0$	DR	207.00	2.04(−20)

3.3. The *K*-shell rate coefficients

In Fig. 6, the calculated rate coefficients for *K*-shell $\Delta n = 1$ ($1s \rightarrow 2l$) resonant recombination of Si^{10+} are compared with the experimental results by Bernhardt *et al.*[30]. Good agreements are obtained. We identify the resonance peaks and find that there is an identification error for the experimental peak in Ref. [30]. The strong states are listed in Table 5. From the table, we can see that the resonance $(1s2s^22p_{1/2}2p_{3/2})_{5/2}$ is the strongest, with the resonance energy $E_d = 1405.10$ eV,

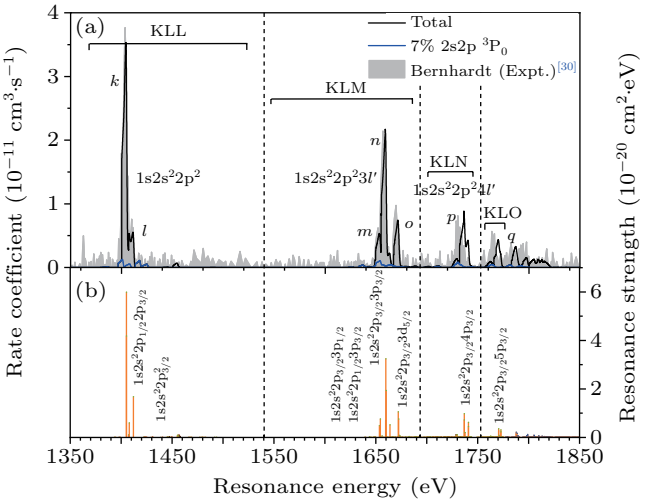


Fig. 6. (a) Comparison of the calculated resonant recombination rate coefficients (black line) for *K*-shell $\Delta n = 1$ transition of Si^{10+} with the experiments results (gray area).[30] The blue lines represent the contributions of the metastable state $2s2p\ ^3P_0$. The strong resonances are also listed in Table 5. The calculated results are considered the contribution of 93% $2s^2\ ^1S_0$ and 7% $2s2p\ ^3P_0$. (b): The resonance strengths from the ground state (orange line). The electron-beam temperatures are $kT_{\parallel} = 0.093$ meV and $kT_{\perp} = 5$ eV in longitudinal and transverse directions.

Table 5. Calculated resonance energies (in eV) and resonance strengths (in cm^2·eV) in the KLL DR of Si^{10+} ions in the ground state. Only the resonance states with $S_d > 1\times10^{-21}$ (cm^2·eV) are tabulated. ($A(B)$ denotes $A\times10^B$).

Peaks	Resonance state	Resonance energy	Resonance strength
k	$((1s2s^22p_{1/2})_1 2p_{3/2})_{5/2}$	1405.10	5.99(−20)
	$((1s2s^22p_{1/2})_0 2p_{3/2})_{3/2}$	1405.20	4.19(−20)
	$((1s2s^22p_{1/2})_1 2p_{3/2})_{1/2}$	1407.20	1.10(−21)
l	$((1s2s^22p^2_{3/2})_{3/2}$	1408.00	6.01(−21)
	$((1s2s^22p^2_{3/2})_{1/2}$	1412.10	1.68(−20)
m	$((1s2s^22p_{1/2})_1 3p_{3/2})_{3/2}$	1653.60	4.87(−21)
	$((1s2s^22p_{3/2})_2 3p_{1/2})_{5/2}$	1654.50	7.66(−21)
n	$((1s2s^22p_{3/2})_1 3p_{1/2})_{3/2}$	1659.60	6.97(−21)
	$((1s2s^22p_{3/2})_1 3p_{3/2})_{5/2}$	1659.80	3.24(−20)
	$((1s2s^22p_{3/2})_1 3p_{3/2})_{3/2}$	1660.10	1.94(−20)
	$((1s2s^22p_{3/2})_1 3p_{3/2})_{1/2}$	1663.90	5.19(−21)
o	$((1s2s^22p_{3/2})_1 3d_{5/2})_{7/2}$	1672.10	1.05(−20)
	$((1s2s^22p_{3/2})_1 3d_{3/2})_{5/2}$	1672.40	7.62(−21)

and resonance strength $S_d = 5.99\times10^{-20}$ cm^2·eV. It is found that for the K-shell $\Delta n = 1$ process, the contribution of the metastable state is negligible.

3.4. Plasma rate coefficient

Figure 7 displays the plasma rate coefficients of Si^{10+} in the ground state $2s^2\ ^1S_0$ (red solid line). It includes the L-shell $2s\rightarrow3l$, $2s\rightarrow4l$, and K-shell $1s\rightarrow2l$ resonant recombinations (black solid lines). For comparison, the experimental result from Bernhardt *et al.* (black dashed lines)[30] and the theoretical result from Gu (blue dash-dotted line)[28] are also plotted. Our calculations are in good agreement with the result from Gu[28] for temperatures $T \leq 1000$ eV. The discrepancies at high temperatures may arise from the additional contributions of the TR and QR processes incorporated in the present calculations. Both our theoretical results and those from Gu[28] are larger than the experimental results reported by Bernhardt *et al.*,[30] within the systematic uncertainty (26%) of the experiment. These discrepancies could be due to collisional cascade processes[42,43] that have not been taken into account in the calculations.

Table 6. Fitting parameters c_i (in cm^3·s^{-1}·eV$^{3/2}$) and E_i (in eV) of plasma rate coefficients for resonant recombination of Si^{10+}. ($A(B)$ denotes $A\times10^B$).

	$2s\rightarrow3l$		$2s\rightarrow4l$		$1s\rightarrow2l$		Total	
i	c_i	E_i	c_i	E_i	c_i	E_i	c_i	E_i
1	−1.746(−12)	1.941	4.728(−10)	361.473	3.928(−09)	1405.764	2.307(−09)	110.414
2	2.466(−09)	111.644	4.728(−10)	361.473	3.995(−09)	1405.490	1.748(−12)	0.158
3	4.032(−08)	265.511	4.679(−10)	361.252	4.313(−09)	1735.829	2.884(−08)	1550.444
4	−1.162(−12)	1.941	4.469(−10)	350.648	4.910(−09)	1405.861	−8.916(−13)	0.129
5	1.148(−08)	196.912	4.357(−10)	299.243	4.332(−09)	1652.316	4.169(−08)	272.207
6	−2.244(−13)	1.942	4.370(−10)	286.801	4.313(−09)	1735.829	−8.564(−13)	0.190
7	3.133(−12)	1.941	4.480(−10)	268.594	4.292(−09)	1632.603	1.341(−08)	197.204

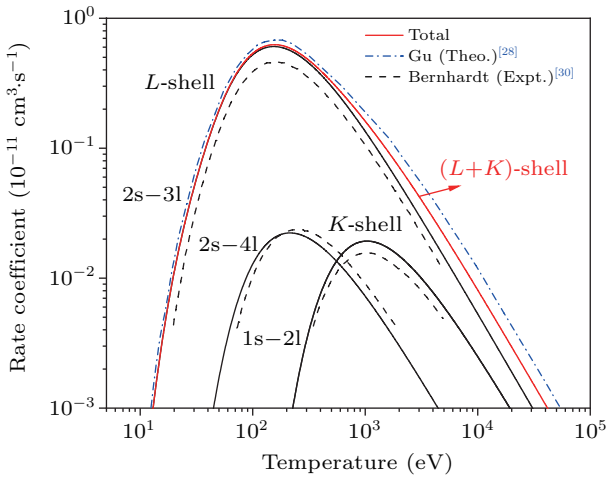


Fig. 7. Comparison of the calculated plasma rates coefficients (solid lines) of Si^{10+} in the ground state ($2s^2\ ^1S_0$) with the TSR measurements (black dashed lines)[30] and theoretical results from Gu (blue dash-dotted lines).[28] The red solid line is the total rate coefficient, and the black solid lines are contributions associated with L-shell $2s\rightarrow3l$, $2s\rightarrow4l$, and K-shell $1s\rightarrow2l$ resonant recombination.

For the convenient use of the calculated results in plasma modeling, the present plasma rate coefficients are fitted with the function[11]

$$\alpha(T_e) = T_e^{-3/2}\sum_i c_i \times \exp\left(-\frac{E_i}{kT_e}\right). \tag{15}$$

The fitting parameters c_i and E_i are summarized in Table 6.

4. Conclusion

Electron-ion resonant recombination of Be-like Si^{10+} forming B-like Si^{9+} in the ground state ($2s^2\ ^1S_0$) and the metastable state ($2s2p\ ^3P_0$) has been systematically studied based on a fully relativistic distorted-wave approximation. Significant resonant recombination channels associated with L- shell $\Delta n = 1$ and 2 ($2s\rightarrow3l$ and $4l$) DR and TR, as well as K-shell $\Delta n = 1$ ($1s\rightarrow2l$) DR, TR, and QR were considered. The present rate coefficients are in excellent agreement with the experimental measurements by Bernhardt *et al.*[30] Moreover, we find that the contributions from the TR process and the metastable state ion are important for the L-shell rate coefficients and cannot be neglected. Finally, plasma recombination rate coefficients are presented in the temperature range

of 10 to 10^5 eV, and convenient analytic fits are provided for modeling astrophysical and fusion plasmas.

Acknowledgments

Project supported by the National Key Research and Development Program of China (Grant No. 2022YFA1602500), the National Natural Science Foundation of China (Grant Nos. 12064041, 11874051, 12104373, 12374384, and 12464036), Central Leading Local Science and Technology Development Fund Projects (Grant No. 23ZYQA293), funds for Innovative Fundamental Research Group Project of Gansu Province (Grant No. 20JR5RA541), and Research and Innovation Project of Gansu University of Political Science and Law (Grant No. GZF2025XQN18).

References

[1] Savin D W, Gwinner G, Grieser M, Repnow R, Schnell M, Schwalm D, Wolf A, Zhou S G, Kieslich S, Müller A, *et al.* 2006 *The Astrophysical Journal* **642** 1275
[2] Schippers S, Schnell M, Brandau C, Kieslich S, Müller A and Wolf A 2004 *Astronomy & Astrophysics* **421** 1185
[3] Zhang C Y, Wu S J, Wang K, Si R, Yao K, Huang Z K, Wen W Q, Ma X W, Chen C Y and Badnell N 2023 *Phys. Rev. A* **108** 022801
[4] Shah C, Amaro P, Steinbrügge R, Bernitt S, López-Urrutia J R C and Tashenov S 2018 *The Astrophysical Journal Supplement Series* **234** 27
[5] Schnell M, Gwinner G, Badnell N, Bannister M, Böhm S, Colgan J, Kieslich S, Loch S, Mitnik D, Müller A, *et al.* 2003 *Phys. Rev. Lett.* **91** 043001
[6] Beilmann C, Mokler P H, Bernitt S, Keitel C H, Ullrich J, López-Urrutia J R C and Harman Z 2011 *Phys. Rev. Lett.* **107** 143201
[7] Beilmann C, Harman Z, Mokler P, Bernitt S, Keitel C, Ullrich J and López-Urrutia J C 2013 *Phys. Rev. A* **88** 062706
[8] Xie L Y, Lu S M, Cheng X S, Zhang D H, Jiang J and Dong C Z 2019 *X-Ray Spectrometry* **48** 657
[9] Xie L Y, Rui J L, Zhang J M, Schuch R and Dong C Z 2022 *Phys. Rev. A* **105** 012823
[10] Dou L J, Xie L Y, Zhang D H, Dong C Z, Wen W Q, Huang Z K and Ma X W 2017 *The European Physical Journal D* **71** 1
[11] Rui J L, Xie L Y, He W L, Ma Y L, Schuch R and Dong C Z 2024 *Phys. Scr.* **99** 125406
[12] Fogle M, Badnell N, Glans P, Loch S, Madzunkov S, Abdel-Naby S A, Pindzola M and Schuch R 2005 *Astronomy & Astrophysics* **442** 757
[13] Orban I, Böhm S, Loch S D and Schuch R 2008 *Astronomy & Astrophysics* **489** 829
[14] Orban I, Loch S D, Böhm S and Schuch R 2010 *The Astrophysical Journal* **721** 1603
[15] Huang Z K, Wen W Q, Xu X, Mahmood S, Wang S X, Wang H B, Dou L J, Khan N, Badnell N R, Preval S P, Schippers S, Xu T H, Yang Y, Yao K, Xu W Q, Chuai X Y, Zhu X L, Zhao D M, Mao L J, Ma X M, Li J, Mao R S, Yuan Y J, Wu B, Sheng L N, Yang J C, Xu H S, Zhu L F and Ma X 2018 *The Astrophysical Journal Supplement Series* **235** 2
[16] Wang S X, Xu X, Huang Z K, Wen W Q, Wang H B, Khan N, Preval S P, Badnell N R, Schippers S, Mahmood S, Dou L J, Chuai X Y, Zhao D M, Zhu X L, Mao L J, Ma X M, Li J, Mao R S, Yuan Y J, Tang M T, Yin D Y, Yang J C, Ma X and Zhu L F 2018 *The Astrophysical Journal* **862** 134
[17] Schippers S, Schmidt E W, Bernhardt D, Yu D, Müller A, Lestinsky M, Orlov D A, Grieser M, Repnow R and Wolf A 2007 *J. Phys.: Conf. Ser.* **58** 137
[18] Orlov D A, Krantz C, Bernhardt D, Brandau C, Hoffmann J, Müller A, Ricsóka T, Schippers S, Shornikov A and Wolf A 2009 *J. Phys.: Conf. Ser.* **163** 012058
[19] Beilmann C, Postavaru O, Arntzen L, Ginzel R, Keitel C, Mäckel V, Mokler P, Simon M, Tawara H, Tupitsyn I, *et al.* 2009 *Phys. Rev. A* **80** 050702
[20] Shah C, Jörg H, Bernitt S, Dobrodey S, Steinbrügge R, Beilmann C, Amaro P, Hu Z, Weber S, Fritzsche S, *et al.* 2015 *Phys. Rev. A* **92** 042702
[21] Shah C, Amaro P, Steinbrügge R, Beilmann C, Bernitt S, Fritzsche S, Surzhykov A, Crespo López-Urrutia J R and Tashenov S 2016 *Phys. Rev. E* **93** 061201
[22] Fletcher L 2024 *Annual Review of Astronomy and Astrophysics* **62** 437
[23] Mancuso S, Giordano S, Barghini D and Telloni D 2020 *Astronomy & Astrophysics* **644** A18
[24] Mernier F, de Plaa J, Pinto C, Kaastra J S, Kosec P, Zhang Y Y, Mao J, Werner N, Pols O R and Vink J 2016 *Astronomy & Astrophysics* **595** A126
[25] Simionescu A, Nakashima S, Yamaguchi H, Matsushita K, Mernier F, Werner N, Tamura T, Nomoto K, De Plaa J, Leung S, *et al.* 2019 *Monthly Notices of the Royal Astronomical Society* **483** 1701
[26] Mernier F, Biffi V, Yamaguchi H, Medvedev P, Simionescu A, Ettori S, Werner N, Kaastra J, de Plaa J and Gu L 2018 *Space Science Reviews* **214** 1
[27] Dufresne R, Del Zanna G and Storey P 2021 *Monthly Notices of the Royal Astronomical Society* **505** 3968
[28] Gu M 2003 *The Astrophysical Journal* **590** 1131
[29] Colgan J, Pindzola M, Whiteford A and Badnell N 2003 *Astronomy & Astrophysics* **412** 597
[30] Bernhardt D, Becker A, Brandau C, Grieser M, Hahn M, Krantz C, Lestinsky M, Novotnỳ O, Repnow R, Savin D W, *et al.* 2016 *J. Phys. B: Atom. Mol. Opt. Phys.* **49** 074004
[31] Cheng K T, Chen M H and Johnson W R 2008 *Phys. Rev. A* **77** 052504
[32] Gu M F 2008 *Canadian Journal of Physics* **86** 675
[33] Pindzola M, Badnell N and Griffin D 1992 *Phys. Rev. A* **46** 5725
[34] Rui J L, Xie L Y, Ma Y L and Dong C Z 2023 *Euro. Phys. J. D* **77** 174
[35] Jönsson P, Godefroid M, Gaigalas G, Ekman J, Grumer J, Li W, Li J, Brage T, Grant I P, Bieroń J, *et al.* 2022 *Atoms* **11** 7
[36] Savelyev I M, Kaygorodov M Y, Kozhedub Y S, Malyshev A V, Tupitsyn I I and Shabaev V M 2023 *Phys. Rev. A* **107** 042803
[37] Hahn Y 1997 *Reports on Progress in Physics* **60** 691
[38] Andersen L H and Bolko J 1990 *Phys. Rev. A* **42** 1184
[39] Schuch R, Barany A, Danared H, Elander N and Mannervik S 1989 *Nuclear Instruments and Methods in Physics Research Section B: Beam Interactions with Materials and Atoms* **43** 411
[40] Behar E, Mandelbaum P and Schwob J 1999 *Phys. Rev. A* **59** 2787
[41] Kramida A, Yu Ralchenko, Reader J and and NIST ASD Team 2023 NIST Atomic Spectra Database (ver. 5.11), [Online], [2024, October 17]. National Institute of Standards and Technology, Gaithersburg, MD.
[42] Hahn Y 1985 *Advances in Atomic and Molecular Physics* vol. 21 (Elsevier) pp. 123–196
[43] McLaughlin D and Hahn Y 1982 *Journal of Quantitative Spectroscopy and Radiative Transfer* **28** 343